



Measurements and predictions of subsidence induced by soil consolidation using persistent scatterer InSAR and a hyperbolic model

Sang-Wan Kim,^{1,2} Shimon Wdowinski,¹ Timothy H. Dixon,¹ Falk Amelung,¹ Jeong Woo Kim,³ and Joong-Sun Won⁴

Received 3 November 2009; revised 11 January 2010; accepted 27 January 2010; published 11 March 2010.

[1] A space-borne SAR interferometric technique is presented for measuring and predicting ground subsidence associated with soil consolidation. Instead of a conventional constant velocity model, a hyperbolic model is introduced for persistent scatterer SAR interferometry (PSI) processing. Twenty three JERS-1 SAR acquired between 1992 and 1998 were used to measure land subsidence in Mokpo city, Korea which had been primarily built on land reclaimed from the sea. Two subsidence field maps were derived and compared: a constant velocity model and a hyperbolic model. Non-linear components depending on the stage of soil consolidation are well represented by the hyperbolic model. The maximum subsidence velocity reaches over 6 cm/yr, while the maximum acceleration is about -0.3 to -0.4 cm/year². The predicted subsidence rate with the new model was validated by using later ENVISAT SAR data for 2004–2005. Prediction accuracy with the non-linear model is improved significantly, indicating the importance of a physically-based deformation model. **Citation:** Kim, S.-W., S. Wdowinski, T. H. Dixon, F. Amelung, J. W. Kim, and J.-S. Won (2010), Measurements and predictions of subsidence induced by soil consolidation using persistent scatterer InSAR and a hyperbolic model, *Geophys. Res. Lett.*, 37, L05304, doi:10.1029/2009GL041644.

1. Introduction

[2] Ground subsidence in urban areas is induced by various processes including a withdrawal of groundwater, oil or natural gas, underground excavation, mining, or tectonic motion [Cabral-Cano *et al.*, 2008; Galloway *et al.*, 1999; Hu *et al.*, 2004]. The land subsidence often results in severe and extensive damage to civil infrastructure. In coastal cities where land elevation is close to sea level, subsidence enhances susceptibility to flooding as shown when New Orleans was flooded during Hurricane Katrina [Dixon *et al.*, 2006].

[3] In urban areas, differential SAR interferometry (DInSAR) and persistent scatterer SAR interferometry (PSI) have been used to monitor ground subsidence. The

PSI technique has been developed more recently and applied to monitor slow but consistent ground subsidence [Ferretti *et al.*, 2001]. PSI has advantages that include fewer limitations with respect to baseline and temporal decorrelation, correction for atmospheric effects, and the ability to generate time series of deformation.

[4] In most PSI applications, surface deformation has been simplified as a temporally linear deformation or a sinusoidal periodic deformation [Colesanti *et al.*, 2003; Ferretti *et al.*, 2000; Kampes and Hanssen, 2004]. However, aquifer system compaction associated with ground water withdrawal, or organic soil drainage, often causes steady but decreasing ground subsidence with time, as compaction limits are reached [Terzaghi, 1925]. In reclaimed land, initially rapid subsidence also decreases with time as the soil consolidation process proceeds. DInSAR was successfully applied to measuring subsidence in reclaimed lands and magnetic extensometer measurements were used for comparison [Kim *et al.*, 2005]. In this study, surface deformation induced by soil consolidation is mapped and predicted by using PSI. Instead of a constant velocity model, we use a hyperbolic model for the PSI measurements and corresponding predictions of soil consolidation. Twenty three JERS-1 SAR images acquired between 1992 and 1998 were used to estimate the land subsidence rate and build a hyperbolic prediction model for the city of Mokpo, Korea. The city is vulnerable to significant subsidence because about 70% of the city area consists of land reclaimed from the sea. The hyperbolic subsidence model is validated by using it to predict subsequent ENVISAT SAR measurements taken during 2004–2005.

2. Method

[5] The phase of topographically corrected interferogram, $\phi_{x,i}$, at the location, x , of the i th interferometric pair is described by:

$$\phi_{x,i} = \phi_{defo,x,i} + \phi_{topo,x,i} + \phi_{const,i} + \phi_{slope,x,i} + \phi_{atm,x,i} + \phi_{noise,x,i}, \quad (1)$$

where ϕ_{const} , ϕ_{slope} and $\phi_{atmosphere}$ (the sum of three components is called APS) are respectively constant phase values, linear phase contributions induced by atmospheric effects and/or orbital fringes, and nonlinear atmospheric effects. The $\phi_{defo,x,i}$ and $\phi_{topo,x,i}$ are phase contributions from ground deformation and DEM error (ϵ) at each ground target, respectively. From selected potential persistent scatterers (PSs) based on amplitude stability or coherence stability, the APS is estimated by means of exploiting time

¹Division of Marine Geology and Geophysics, University of Miami, Miami, Florida, USA.

²Department of Geoinformation Engineering, Sejong University, Seoul, South Korea.

³Department of Geomatics Engineering, University of Calgary, Calgary, Alberta, Canada.

⁴Department of Earth System Sciences, Yonsei University, Seoul, South Korea.

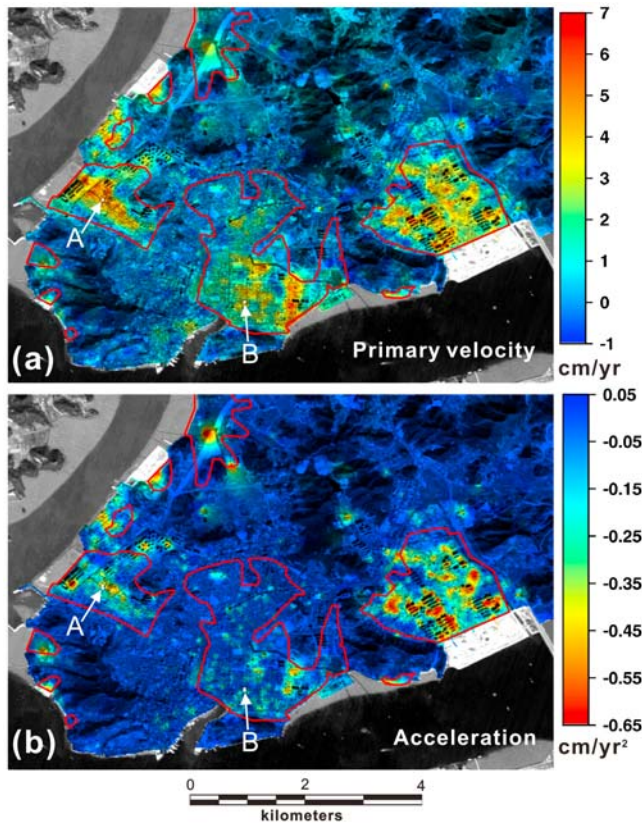


Figure 1. Subsidence map of Mokpo city derived by means of JERS-1 PS analysis using hyperbolic model. (a) Primary velocity and (b) acceleration term at the PSs calculated from equation (4). Both maps were calculated on regular spatial grid by means of Kriging interpolation. Background image is optical satellite image, and red polygon represents the main reclaimed area. The temporal evolution of the deformation at two PSs marked by A and B are shown in Figure 2.

series of phase value. The estimated APS is interpolated spatially and then subtracted from each differential interferogram. A detailed description of PSI algorithm is given by *Colesanti et al.* [2003] and *Ferretti et al.* [2001].

[6] After removing APS, ground deformation and DEM errors are computed on a pixel-by-pixel basis in a multi-interferogram framework. DEM error is proportional to the perpendicular component of baseline, while surface displacement is a function of time. One of the key issues is a selection of a mathematical model accounting for target motion. A constant velocity model ($\phi_{defo,x,i} = 4\pi/\lambda \cdot v \cdot t_i$, where λ : wavelength, v : velocity, t_i : time interval with respect to the reference image) which is most commonly adopted as a physical model for ground subsidence is not adequate for our study because the subsidence induced by soil consolidation is not a constant in time. Here we introduce a hyperbolic model because it is widely used by engineers for settlement prediction due to soil consolidation [*Kim et al.*, 2005; *Tan et al.*, 1991].

[7] The observed phase of each PS (x) at each time (i) is modeled as:

$$\phi_{defo,x,i} = \frac{4\pi}{\lambda} \frac{t_i}{v_a + v_b t_i}, \quad (2)$$

where t_i is a time interval with respect to the reference image, and v_a and v_b are site specific constants constrained by time-series phase measurements. When v_b is zero in the equation (2), it represents a constant velocity model (or a linear subsidence model) whose velocity is $1/v_a$. Three unknown parameters, v_a , v_b , and ε (DEM error) can be solved by maximizing the following equation in three-dimensional model space:

$$\Gamma(v_a, v_b, \varepsilon) = \left| \frac{1}{n} \sum_{i=1}^n e^{j(\phi_{x,i} - \phi_{defo,x,i} - \phi_{topo,x,i})} \right|, \quad (3)$$

$n = \text{the number of pairs.}$

The phase coherence (Γ), ranging from 0 to 1, is considered as a reliability measure in fitting a deformation model. Since the uncertainty of estimated parameters increases as the number of unknown parameters increases, we need a large number of dataset or to limit the range of time variable velocity, v_b , based on a prior knowledge of the displacement velocity.

[8] An approximation to the hyperbolic model of equation (2) can be derived by a Taylor series to obtain

$$\begin{aligned} Defo(t) &= f(t_c) + (t - t_c) \cdot f'(t_c) + \dots \\ &= \frac{1}{v_a}(t - t_c) - \frac{v_b}{v_a^2}(t - t_c)^2 + \dots \end{aligned} \quad (4)$$

The first term on the right-hand side, $1/v_a$, is considered as a primary velocity or constant velocity term as the average velocity throughout the time series in the middle of observation period, t_c . The second term, v_b/v_a^2 , is a linear velocity rate (or a acceleration). By introducing the approximation, we can separate a quadratic subsiding component from the conventional linear component, which is useful for visual display of the hyperbolic model results.

3. Application Results

3.1. Data Set and Processing

[9] The hyperbolic model algorithm was applied to the city of Mokpo ($\sim 5 \times 5$ km) located on the south western coast of Korea. Large areas within the city are subjected to significant subsidence caused by soil consolidation, because the city was built on a land reclaimed from the sea since the early 1920s. The distribution of reclaimed area is shown in Figure 1. Due to rapid subsidence, several places in the city have suffered significant damages in the past.

[10] The JERS-1 L-band SAR satellite acquired a significant number of data over the Korean Peninsula. We obtained twenty three JERS-1 SAR scenes (path: 88, row: 242) from September 1992 to October 1998. Twenty two interferograms were formed with respect to a reference image acquired on March 24, 1996, which was selected by considering spatial baselines and time intervals. Maximum perpendicular baseline component was about 3 km. Because of inaccurate orbit information for JERS-1, a baseline optimization was performed before PSI application. The inaccurate baseline of JERS-1 SAR was corrected by using the digital elevation model (DEM) and removing long wavelength's residual fringe. To remove the topographic contribution in the interferometric phase, the SRTM 3-arc DEM (~ 90 -m spacing) was used. After eliminating APS using

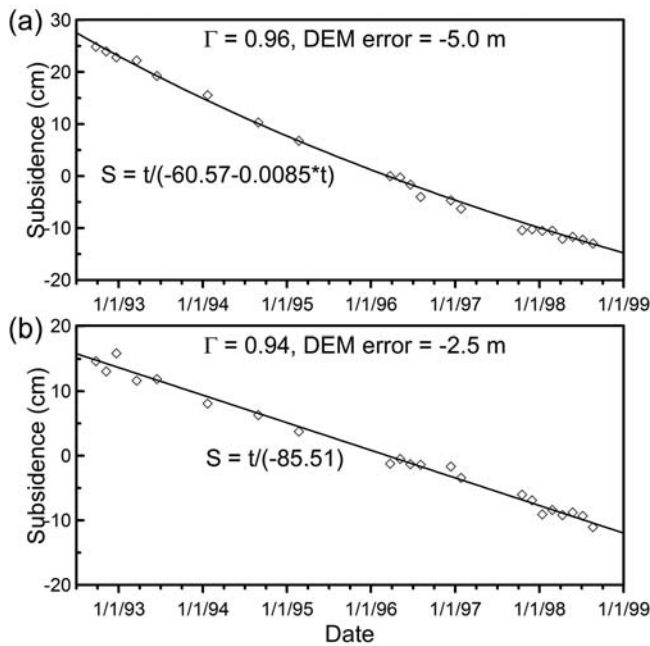


Figure 2. Temporal behaviors of the subsidence measured at two selected (a) point A and (b) point B in Figure 1. Hyperbolic model solutions for deformation estimated from PSI method are also displayed. Note that the model parameter v_b (see equation (2)) at the point B is zero, consequently the model solution is identical with the linear model. Temporal coherence Γ and DEM error estimated during PSI processing are presented in the plots.

initially selected permanent scatterers (13 points per km^2), we applied both a constant velocity model and a hyperbolic model to measure and predict soil consolidation rates. Two parameters (DEM errors and constant velocity) for the linear model or three parameters (DEM errors, v_a and v_b) for the hyperbolic model (see equation (2)) are estimated at each pixel using the periodogram.

3.2. Deformation Field From PSI

[11] PSs ($\Gamma \geq 0.8$) with an average density of $371/\text{km}^2$ were obtained in Mokpo city, then a two-dimensional subsidence velocity and velocity change fields were estimated by interpolating and low-pass filtering measurements at the PSs (Figure 1). These maps allow a time-varying description of velocity. Figure 1a shows the detailed subsidence patterns. Significant subsidence occurred in most of the reclaimed coastal areas. Major subsiding areas are confined to the northwestern, southern and eastern part of the study area. The primary velocity is similar to PSI measurement with conventional constant velocity model [Kim *et al.*, 2008]. All three areas are densely populated residential districts in the city of Mokpo. Estimated maximum subsidence rate reaches about 6 cm/yr in each zone. Building damage and road subsidence have been frequently reported in these areas during 1990s and 2000s.

[12] The time dependent component of the model (Figure 1b) enables us to predict the non-linear behavior of subsidence. Subsidence in the eastern and northwestern parts has a large time-varying velocity, with rate changes ~ 0.3 to -0.4 cm/year^2 ($\sim 10\%$ contribution of primary

velocity). The time-varying velocity term in the southern part is insignificant. This may reflect different sediment types in the underlying tidal flats or different degree of loaded soil compaction.

[13] PSI provides deformation components at each SAR acquisition time, so a complete evolution of the deformation can be estimated for each coherent pixel. In order to demonstrate the capability of the hyperbolic model to detect the temporal evolution of the deformation in a time-varying velocity field, we selected two PSs with different time-varying components, marked by A and B in Figure 1. Figure 2 presents temporal deformation series for two PSs as well as solutions of the hyperbolic model. For the point A, temporal ensemble coherence is 0.96 and two parameters (v_a and v_b) for velocity model in equation (2) are about -60.6 day/cm and -0.0085 1/cm. Temporal coherence and two parameters for the point B are 0.94, and -85.5 cm/day and 0 cm/day^2 , respectively. Note that the model parameter v_b at the point B is zero, consequently the result equals the solution of the linear model. The subsidence velocity at point A tends to significantly decrease with time. Although the primary subsidence rate (or mean subsidence rate) at point A during the SAR observations is larger than point B the future subsidence would be quite different due to the different time-varying velocity component. Considering the models displayed in Figure 2 the subsidence velocity at the point A will be less than the point B after December 1999. This effect would be evident in any subsidence analysis conducted after 2000.

3.3. Verification of Predicted Deformation

[14] Ground truth data are unfortunately unavailable even though the subsidence has been consistently reported in the study area while ENVISAT SAR datasets were acquired along descending orbits in the time span from 2004 to 2005. Therefore we explored displacement values derived from ENVISAT interferograms, then compared them to model calculations based on the previous PSI results based on JERS-1 data from 1992–1998 (see Figure 1). Figure 3a presents subsidence calculated from ENVISAT interferometric pair (31 Oct 2004 – 11 Sep 2005) with a time span of 315 days. Displacements for radar line-of-sight (LOS) direction of ENVISAT are converted to subsidence values taking into account incidence angle of 24.8° under the assumption of pure vertical movements. Although the incidence angle between JERS and ENVISAT measurements differ by 12.5° , the measurement errors related to the incidence angle difference can be disregarded because the horizontal component error budget is less than 20% ($= \sin 37.3^\circ - \sin 24.8^\circ$). In any case soil consolidation is expected to dominate the subsidence in the study area.

[15] Both the linear model (i.e., constant velocity) and hyperbolic model were used for the comparison. Using these two models, we calculated the expected soil consolidation during the time span of ENVISAT data acquisitions (Figures 3c and 3e). The southern area shows similar deformation values in the two model results because the time-varying component of deformation is not significant (see Figure 1b). Conversely, large differences of deformation predicted by the two models are evident in the northwestern area, where the time-varying component is large. Residual maps (Figures 3d and 3f) between ENVISAT

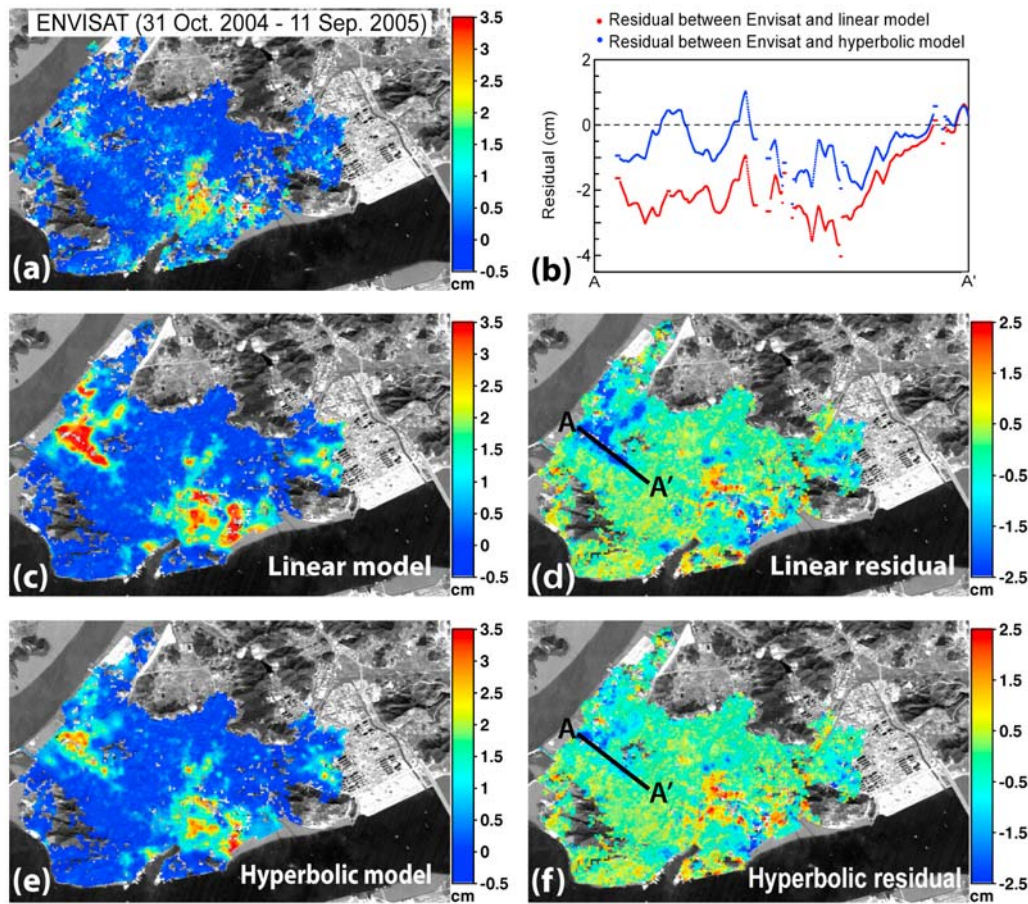


Figure 3. Comparison between linear model and hyperbolic model using ENVISAT measurement. (a) Subsidence derived from ENVISAT InSAR pair (31 Oct. 2004 and 11 Sep. 2005), (b) two model's residual deformation at profile A-A', (c and d) linear model and residual for the subsidence during the ENVISAT observation, (e and f) hyperbolic model subsidence and residual. The subsidence from 2004–2005 is better described by a hyperbolic model.

observation and two models clearly show significant improvement in hyperbolic model in terms of a prediction of subsidence due to soil consolidation. Figure 3b displays residuals of the two models along the profile A-A'. While deviations from the hyperbolic model (blue line) are less than 1 cm, those from constant velocity model (red line) are larger and exceed 2 cm in some parts. The mean and standard deviation of the residuals are summarized in Table 1. Significant improvements are evident in the northwestern area. The residual means were improved from -1.0 cm to -0.5 cm, and the standard deviations decreased from 1.1 cm to 0.7 cm. For the overall area, the hyperbolic model shows better results than the linear model. In summary, the hyperbolic model in association with PSI measurements

more effectively predicts soil consolidation than the conventional constant velocity model.

4. Conclusions

[16] Subsidence induced by soil consolidation in Mokpo city, Korea during 1992–1998 was estimated using the JERS-1 PSI. A hyperbolic model was adopted as the priori model for the relative phase of persistent scatterer, and compared to a more conventional constant velocity model. The hyperbolic model is composed of a linear displacement and time-varying component of deformation. The primary velocity component of hyperbolic model agrees well with the constant velocity model. The time-varying component is

Table 1. Mean and Standard Deviation of Residual Errors Between Envisat Subsidence Maps and Subsidence Estimations Predicted From JERS-1 PSI Results Using Hyperbolic and Linear Models

Model	Overall Area		Southern Area		Northwestern	
	Mean Velocity (cm)	STD (cm)	Mean Velocity (cm)	STD (cm)	Mean Velocity (cm)	STD (cm)
Linear model	-0.29	0.88	-0.20	0.89	-0.97	1.08
Hyperbolic model	-0.11	0.68	0.01	0.79	-0.50	0.69

associated with aquifer system compaction and slow deceleration of ground subsidence. The result was validated by using ENVISAT SAR measurements acquired during 2004–2005.

[17] By exploiting a hyperbolic model, we are able to more precisely predict future subsidence, as well as to build a better velocity field during the period of SAR observation. We conclude that the PSI technique coupled with a hyperbolic model is a valuable tool for monitoring long-term land subsidence characterized by time varying subsidence rate, which may be characteristic of soil consolidation or aquifer system compaction. The derived settlement map can be used for defining and forecasting possible hazard zones associated with subsidence.

[18] **Acknowledgments.** We thank NASA and ONR for support. The research was supported by the National Research Lab. Project (M1-0302-00-0063) of Korea Ministry of Science and Technology. This work was also supported by the Korea Research Foundation grant (KRF-2009-013-C00051). CSTARS contribution 26.

References

- Cabral-Cano, E., T. H. Dixon, F. Miralles-Wilhelm, O. Diaz-Molina, O. Sanchez-Zamora, and R. E. Carande (2008), Space geodetic imaging of rapid ground subsidence in Mexico City, *Geol. Soc. Am. Bull.*, *120*(11–12), 1556–1566.
- Colesanti, C., A. Ferretti, F. Novali, C. Prati, and F. Rocca (2003), SAR monitoring of progressive and seasonal ground deformation using the permanent scatterers technique, *IEEE Trans. Geosci. Remote Sens.*, *41*(7), 1685–1701.
- Dixon, T. H., F. Amelung, A. Ferretti, F. Novali, F. Rocca, R. Dokka, G. Sella, S. W. Kim, S. Wdowinski, and D. Whitman (2006), Subsidence and flooding in New Orleans, *Nature*, *441*(7093), 587–588.
- Ferretti, A., C. Prati, and F. Rocca (2000), Nonlinear subsidence rate estimation using permanent scatterers in differential SAR interferometry, *IEEE Trans. Geosci. Remote Sens.*, *38*(5), 2202–2212.
- Ferretti, A., C. Prati, and F. Rocca (2001), Permanent scatterers in SAR interferometry, *IEEE Trans. Geosci. Remote Sens.*, *39*(1), 8–20.
- Galloway, D. L., D. R. Jones, and S. E. Ingebritsen (1999), Land subsidence in the United States, *U.S. Geol. Surv. Circ.*, *1182*.
- Hu, R. L., Z. Q. Yue, L. C. Wang, and S. J. Wang (2004), Review on current status and challenging issues of land subsidence in China, *Eng. Geol.*, *76*(1–2), 65–77.
- Kampes, B. M., and R. F. Hanssen (2004), Ambiguity resolution for permanent scatterer interferometry, *IEEE Trans. Geosci. Remote Sens.*, *42*(11), 2446–2453.
- Kim, S. W., C. W. Lee, K. Y. Song, K. D. Min, and J. S. Won (2005), Application of L-band differential SAR interferometry to subsidence rate estimation in reclaimed coastal land, *Int. J. Remote Sens.*, *26*(7), 1363–1381.
- Kim, S. W., S. Wdowinski, T. H. Dixon, F. Amelung, J. S. Won, and J. W. Kim (2008), InSAR-based mapping of surface subsidence in Mokpo City, Korea, using JERS-1 and ENVISAT SAR data, *Earth Planets Space*, *60*(5), 453–461.
- Tan, T. S., T. Inoue, and S. L. Lee (1991), Hyperbolic method for consolidation analysis, *J. Geotech. Eng.*, *117*(11), 1723–1737.
- Terzaghi, K. (1925), Principles of soil mechanics: IV. Settlement and consolidation of clay, *Eng. News Rec.*, *95*(3), 874–878.
- F. Amelung, T. H. Dixon, S.-W. Kim, and S. Wdowinski, Division of Marine Geology and Geophysics, University of Miami, Miami, FL, 33149-1098, USA. (skim@rsmas.miami.edu)
- J. W. Kim, Department of Geomatics Engineering, University of Calgary, 2500 University Dr. NW, Calgary, AB T2N 1N4, Canada.
- J.-S. Won, Department of Earth System Sciences, Yonsei University, 134 Shinchon-dong, Seodaemun-gu, Seoul 120-749, South Korea.